THE ASTROPHYSICAL JOURNAL, 445:716–730, 1995 June 1

MORPHOLOGY, NEAR-INFRARED LUMINOSITY, AND MASS OF THE GALACTIC BULGE FROM *COBE* DIRBE OBSERVATIONS

E. DWEK,[1] R. G. ARENDT,[2] M. G. HAUSER,[5] T. KELSALL,[1] C. M. LISSE,[3] S. H. MOSELEY,[1]
R. F. SILVERBERG,[1] T. J. SODROSKI,[2] AND J. L. WEILAND[4]
Received 1994 June 8; accepted 1994 December 6

ABSTRACT

Near-infrared images of the Galactic bulge at 1.25, 2.2, 3.5, and 4.9 μm obtained by the Diffuse Infrared Background Experiment (DIRBE) onboard the *Cosmic Background Explorer* (*COBE*) satellite are used to characterize its morphology and to determine its infrared luminosity and mass. Earlier analysis of the DIRBE observations (Weiland et al. 1994) provided supporting evidence for the claim made by Blitz & Spergel (1991) that the bulge is bar-shaped with its near end in the first Galactic quadrant. Adopting various triaxial analytical functions to represent the volume emissivity of the source, we confirm the barlike nature of the bulge and show that triaxial Gaussian-type functions provide a better fit to the data than other classes of functions, including an axisymmetric spheroid. The introduction of a "boxy" geometry, such as the one used by Kent, Dame, & Fazio (1991) improves the fit to the data. Our results show that the bar is rotated in the plane with its near side in the first Galactic quadrant creating an angle of $20° \pm 10°$ between its major axis and the line of sight to the Galactic center. Typical axis ratios of the bar are $\{1{:}0.33 \pm 0.11{:}0.23 \pm 0.08\}$, resembling the geometry of prolate spheroids. There is no statistically significant evidence for an out-of-plane tilt of the bar at 2.2 μm, and marginal evidence for a tilt of $\approx 2°$ at 4.9 μm. The introduction of a roll around the intrinsic major axis of the bulge improves the "boxy" appearance of some functions.

A simple integration of the observed projected intensity of the bulge gives a bulge luminosity of 1.2×10^9, 4.1×10^8, 2.3×10^8, and 4.3×10^7 $L_\odot$, respectively, at 1.25, 2.2, 3.5, and 4.9 μm wavelength for a Galactocentric distance of 8.5 kpc. The 2.2 μm luminosity function of the bulge population in the direction of Baade's window yields a bolometric luminosity of $L_{\rm bol} = 5.3 \times 10^9$ $L_\odot$. Stellar evolutionary models relate this luminosity to the number of main-sequence progenitor stars that currently populate the red giant branch. Combined with the recent determination of the main-sequence turnoff mass for the bulge by the *Hubble Space Telescope* (Holtzman et al. 1993) we derive a photometrically determined bulge mass of $\approx 1.3 \times 10^{10}$ $M_\odot$ for a Salpeter initial mass function extended down to 0.1 $M_\odot$.

Subject headings: Galaxy: structure — infrared: stars — Galaxy: stellar content

1. INTRODUCTION

The Diffuse Infrared Background Experiment (DIRBE) onboard the *Cosmic Background Explorer* (*COBE*) satellite has provided striking new images of the Galactic bulge at effective wavelengths of 1.25, 2.2, 3.5, and 4.9 μm (Hauser 1993, Plate 3; Arendt et al. 1994; Weiland et al. 1994). The bulge, defined here as the spheroid within the $|l| < 20°$ and $|b| < 10°$ region around the Galactic center, and its stellar content have been subjects of considerable interest since they contain important clues about the dynamical and star-formation history of our Galaxy. The morphology of the Galactic bulge is much harder to ascertain than that of bulges in many external galaxies, because of our location in the Galactic plane amid the obscuration by interstellar dust. In spite of this difficulty, there has recently been an accumulating body of evidence that the stellar distribution in the bulge is bar-shaped, i.e., that the bulge is not rotationally symmetric in the plane of the disk (see Blitz 1993 for a review of the subject). The existence of a bar in our Galaxy would have important implications for the dynamics of the Galaxy. A bar would provide a mechanism for sweeping gas from the disk into the Galactic center "feeding" a central black hole (e.g., Shlosman, Frank, & Begelman 1989). It would also provide a mechanism for generating spiral arms, and a basis for estimating the mass of the halo relative to that of the disk (e.g., Combes & Sanders 1981 and references therein).

The evidence for a bar at the Galactic center is drawn from (1) stellar and gas dynamics in the Galactic center region (Liszt & Burton 1980; Bahcall, Schmidt, & Soneira 1982; Vietri 1986; Binney et al. 1991; de Zeeuw 1992; Binney & Gerhard 1993); (2) asymmetries in the photometric image of the bulge (Blitz & Spergel 1991, based on the 2.4 μm image obtained by Matsumoto et al. 1982; and Weiland et al. 1994, from DIRBE images at 1.25, 2.2, 3.5, and 4.9 μm); (3) the analysis of stellar tracers of the large-scale Galactic structure (Habing et al. 1985; Rowan-Robinson & Chester 1987; Blanco 1988; Nakada et al. 1991; Whitelock & Catchpole 1992; Weinberg 1992a, b); (4) the excess of gravitational microlensing events in the direction of the Galactic bulge over earlier theoretical expectations (Paczyński et al. 1994); (5) the presence of a hotspot off-center from the Galactic center in the 1.8 MeV COMPTEL sky map (Chen, Gehrels, & Diehl 1994); and (6) the asymmetric distribution of bulge red clump stars detected by the OGLE project (Optical Gravitational Lensing Experiment; Stanek et al. 1994). However, the exact morphology of the bar, its orientation with respect to the disk, and its total bolometric luminosity and mass are still issues that need to be resolved.

[1] Code 685, NASA/Goddard Space Flight Center, Greenbelt, MD 20771.
[2] Applied Research Corporation, Code 685.3, NASA/GSFC, Greenbelt, MD 20771.
[3] Hughes STX, Code 685.9, NASA/GSFC, Greenbelt, MD 20771.
[4] General Sciences Corporation, Code 685.3, NASA/GSFC, Greenbelt, MD 20771.
[5] Code 680, NASA/Goddard Space Flight Center, Greenbelt, MD 20771.

In addition to study of the morphology of the bulge, a significant amount of effort has been expended to determine the stellar content of a select, relatively dust-free, region located at ($l = 1°$, $b = -3°.9$), known as Baade's window. Much of this work is summarized by Frogel (1988) and Rich (1992). Aspects of these observations that are pertinent to our study include the characterization of the bulge population, and the K-band (2.2 μm) luminosity function. The K-band luminosity function is required to convert the 2.2 μm bulge luminosity to a bolometric luminosity. This luminosity can then be used in conjunction with *HST* observations of the bulge turnoff mass (Holtzman et al. 1993) to infer the mass of the bulge K and M giant stars, and, with the aid of stellar evolution theory, to infer the total mass of bulge stars.

The DIRBE images of the Galactic center region provide a new, and much improved data base, in terms of spatial and simultaneous wavelength coverage, and in sensitivity, for studying the bulge. After the subtraction of radiation scattered and emitted by interplanetary dust and emission from the galactic disk, and including a correction for interstellar extinction, the DIRBE data show a longitudinal asymmetry in the intensity maps of the bulge, and a flattening of the light distribution in the north and south polar regions of the bulge, giving it a "boxy" appearance (see Weiland et al. 1994 for a detailed description of the unveiling of the bulge morphology).

In this paper we present an analysis of the DIRBE observations to determine the bulge morphology, luminosity, and mass. The observations, the uncertainties in the data, and the observed characteristics of the light distribution and its asymmetry are described in § 2. The mathematical formalism used in the paper is presented in § 3, and the various functional forms (symmetric and triaxial) used to characterize the light distribution of the bulge are summarized in § 4. The resulting bulge morphology is presented in § 5, and in § 6 we derive the bulge luminosity in the various DIRBE bands, its bolometric value, and the bulge photometric mass. The results of this paper, and comparisons with previous investigations, are briefly summarized in § 7.

2. THE OBSERVATIONS

2.1. *The Bulge Data*

The 1.25, 2.2, 3.5, and 4.9 μm data used in this investigation are a specially processed subset of the DIRBE data consisting of DIRBE weekly averaged maps, selected at 2 week intervals over a 6 month period to achieve complete sky coverage (Weiland et al. 1994). The calibration applied is preliminary, and the same as that used in the publicly released DIRBE Galactic Plane Maps. Each map pixel was observed at a multitude of solar elongations between 64° and 124°. The observations in each celestial direction were interpolated to yield the resulting pixel intensity as it is seen through the interplanetary dust cloud at 90° solar elongation. This interpolation procedure removes the variation of the interplanetary dust scattering and emission with elongation, leaving an almost time-independent component of this signal in the data. A simple empirical model describing the intensity of this component (Hauser 1993) was then subtracted from the data, producing Galactic plane maps which are essentially free of contributions from interplanetary dust emission and scattering.

Assuming that the galactic stellar population is characterized by a single $I(1.25\ \mu m)/I(2.2\ \mu m)$ color ratio, Arendt et al. (1994) showed that the extinction in the central part of the Galaxy can be understood as stellar background sources seen through up to 3.8 optical depths at 1.25 μm of foreground extinction. At 4.9 μm, the extinction toward the Galactic center is reduced to an optical depth of 0.3. Adopting this simple extinction geometry, Arendt et al. created a 1.25 μm extinction map from the observed 1.25 μm and 2.2 μm intensity maps. The Rieke-Lebofsky (1985) reddening law was then used to create extinction maps at 3.5, and 4.9 μm. By construction, the 1.25 and 2.2 μm extinction-corrected maps of the Galaxy are identical to within a multiplicative constant. At Galactic latitudes below $\sim 3°$, the assumption that the extinction arises mainly from foreground material breaks down, as sources are intermixed with the absorbing dust. The extinction correction becomes then highly model dependent, since different wavelengths sample different distrances of the Galactic plane. At 3.5 and 4.9 μm an additional problem prevents the construction of low-latitude extinction maps, namely, the contribution of H II regions and stochastically heated dust to the emission at these wavelengths. For these reasons we have excluded all data at $|b| < 3°$ at 1.25 and 2.2 μm, and at $|b| < 2°$ at 3.5 and 4.9 μm, from the model-fitting procedure. Detailed model results will be presented only at 2.2 μm since they allow for direct comparison of our results with previous efforts that were based on the 2.4 μm map of the bulge obtained by Matsumoto et al. (1982), or by the *Spacelab 2* Infrared Telescope (IRT; see Kent, Dame, & Fazio 1991).

As a final step in preparing the data for comparison with bulge models, the emission of the Galactic disk was removed from the region of interest using the procedure outlined by Weiland et al. (1994). This consisted of making a local empirical fit to the extinction-corrected data for $|l| \leq 90°$, and $|b| \leq 10°$ of the form: $I(l, b) = I_0(b) \exp[-|l|/l_0(b)]$. where $l_0(b)$ increases smoothly with $|b|$ (see Weiland et al. 1994 for details). Positions at positive and negative latitudes were fitted separately, allowing for a latitudinal asymmetry in the Galaxy. Figures 1*a*–1*c* depict the intensity of the Galactic bulge at 2.2, 3.5, and 4.9 μm, largely free of any contaminating zodiacal or Galactic disk emission.

2.2. *Uncertainty Estimates*

To measure how well the various analytical functions represent the volume distribution of bulge sources we need to know the uncertainties in the data. There are various sources contributing to the uncertainty: (1) the removal of the Galactic disk; (2) the extinction corrections (Arendt et al. 1994); (3) the interplanetary dust model (Weiland et al. 1994); (4) systematic errors in the photometric calibration; (5) various noise sources including detector and pixelization noise; and (6) confusion due to point sources superposed on the smooth unresolved emission of the Galactic bulge.

Confusion is the dominant source of error in the data and to quantify it we measured the deviations (σ) between a smoothed map and the map containing *the bulge and the disk* as seen through a foreground of nearby stars. This was done by measuring the deviation of each $0°.32 \times 0°.32$ pixel from the weighted mean of a 9×9 pixel area centered on the pixel to form a "noise" map of the data. The 9×9 pixel area represents the largest size that is not affected by the intrinsic structure of the bulge, and is larger than the 3×3 pixel area over which DIRBE pixels are correlated. The absolute magnitudes of the deviations in the "noise" map were found to be correlated with intensity. In particular we found that the deviations

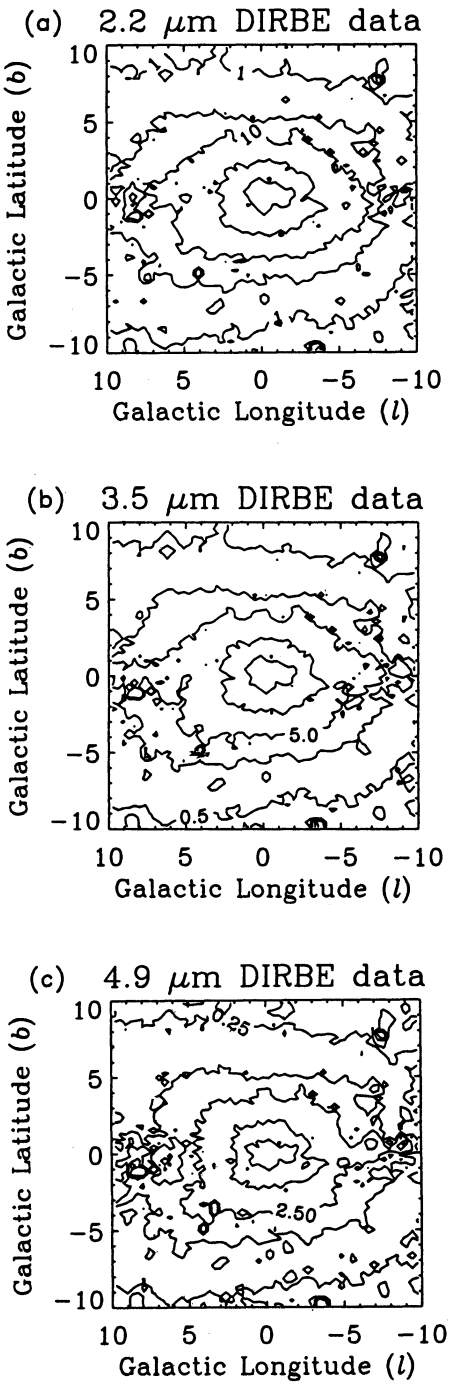

FIG. 1.—Contour maps of the bulge region at (*a*) 2.2 μm; (*b*) 3.5 μm; and (*c*) 4.9 μm, as observed by the DIRBE, after removal of the zodiacal emission, the Galactic disk emission, and after correcting for extinction (see text for details). Contour levels are in units of MJy sr^{-1}.

were distributed in a nearly Gaussian manner about the relation $\sigma = 0.23I^{0.534}$ at 2.2 μm, where σ and I are in units of MJy sr^{-1}. This relation was used to estimate the noise in the intensity of the bulge at each pixel. Typical uncertainties at 2.2 μm are on the order of 0.1 MJy sr^{-1}. Similar relations applied at 3.5 and 4.9 μm, and the same procedure was used to estimate the pixel noise at these wavelengths.

The other sources of uncertainty—the removal of the Galactic disk, the extinction correction, and the removal of the interplanetary dust emission—are systematic in nature and may affect the projected morphology of the bulge. The effect of these uncertainties on our results can be assessed only when more sophisticated models for the Galactic disk and interplanetary dust emission are available.

3. MATHEMATICAL FORMALISM

The calculated intensity of light from the bulge region in the (l, b) direction, $I(l, b)$, is given by an integral of the volume emissivity of the sources, $\rho_s(x, y, z)$, along the line of sight s:

$$I(l, b) = \frac{1}{4\pi}\int_0^\infty \rho_s(x, y, z)ds\,, \qquad (1)$$

where the intensity $I(l, b)$ is in units of flux per steradian. We chose a right-handed coordinate system $\{x, y, z\}$, centered on the Galactic center, with the plane of the sky projected on the xz-plane to describe the geometry of the system. In this system, the positive x-axis points toward decreasing Galactic longitude, the positive z-axis points to Galactic north, and the y-axis increases away from the observer located at $\{x, y, z\} = \{0, -D, 0\}$, where $D = 8.5$ kpc is the adopted distance to the Galactic center. The coordinates $\{x, y, z\}$ are related to the line-of-sight distance s from the observer by: $x = -s\cos(b)\sin(l)$; $y = -D + s\cos(b)\cos(l)$; and $z = s\sin(b)$.

We will assume that the distribution $\rho_s(x, y, z)$ can be described by an analytical function $\rho_{\rm fun}$ subjected to three consecutive rotations: the first, represented by the matrix $R(\alpha)$, is a counterclockwise rotation by an angle α around the z-axis, giving rise to a longitudinal asymmetry in $I(l, b)$; the second, represented by the matix $R(-\beta)$, is a clockwise rotation by an angle β around the new y'-axis, tilting the source distribution out of the Galactic plane and giving rise to both longitudinal and latitudinal asymmetries in $I(l, b)$; the third, represented by the matrix $R(\gamma)$ consists of a roll, defined here as a counterclockwise rotation of the bar around the new x''-axis. Such a rotation is degenerate for prolate spheroids, but will change the projected intensities for triaxial systems. To summarize, $\rho_s(x, y, z) = \rho_{\rm fun}(x''', y''', z''')$, where $\{r'''\} \equiv \{x''', y''', z'''\}$ is related to $\{r\} \equiv \{x, y, z\}$ by $\{r'''\} = R(\gamma)R(-\beta)R(\alpha)\{r\}$. A schematic presentation of our notation convention is given in Figure 2.

4. BAR MODELS AND THEIR CHARACTERISTICS

4.1. *An Oblate Spheroid Model*

Before resorting to triaxial models, it is of interest to see to what extent the bulge can be approximated by an axisymmetric distribution of sources such as an oblate spheroid. Such a simple model will provide first-order estimates of the bulge luminosity, and of the minor-to-major axis ratio of the system. The latter quantity is of great interest, since it contains clues to the dynamical history of the formation of the bulge (Statler 1987; Combes & Sanders 1981; Combes et al. 1990; Raha et al. 1991; Sellwood 1993). We therefore adopt a Gaussian-type function (hereafter referred to as model G0): $\rho = \rho_0 \exp[-0.5r^2]$, where

$$r^2 = \frac{x^2 + y^2}{R_0^2} + \frac{z^2}{z_0^2}\,,$$

to describe the source density distribution in the bulge. R_0 is the scale length of the major axis in the plane of the Galaxy,

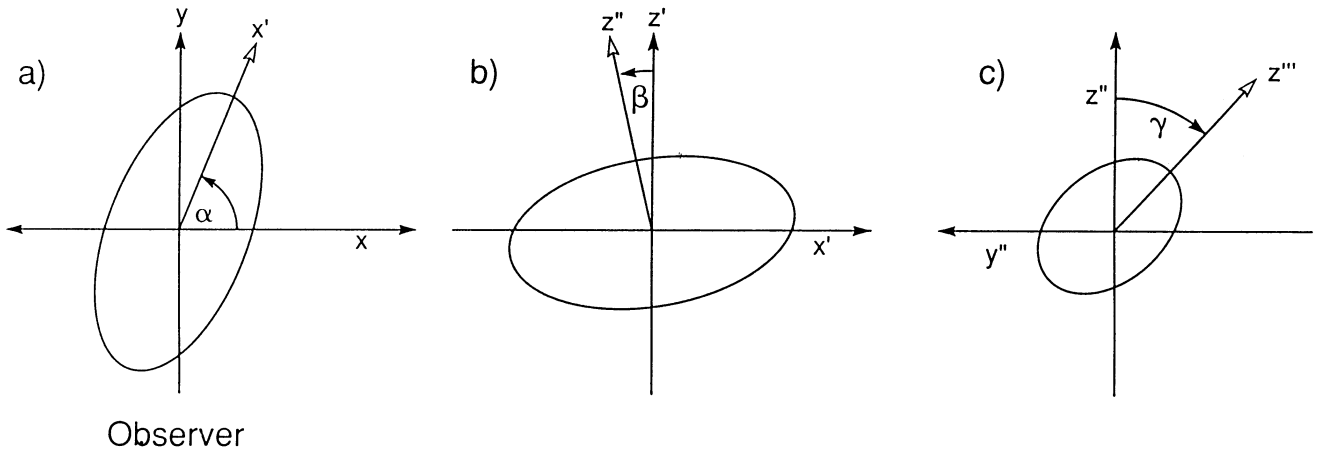

FIG. 2.—Schematic figure of the bulge illustrating the notation convention used in this paper. See § 3.1 for more details.

and z_0 is the scale length of the minor axis in the perpendicular direction. Using equation (1), the apparent intensity of this density distribution as seen by an observer located at a distance D from the Galactic center is given by

$$I(l, b) = \frac{1}{\sqrt{8\pi}} \frac{R_0}{\mathscr{A}_1} \rho_0 \exp\left\{-\frac{1}{2}\left[\left(\frac{D}{R_0}\right)^2 - \mathscr{A}_2^2\right]\right\}, \quad (2)$$

where

$$\mathscr{A}_1 = \sqrt{\cos^2(b) + \left(\frac{R_0}{z_0}\right)^2 \sin^2(b)},$$

$$\mathscr{A}_2 = \left(\frac{D}{R_0}\right)^2 \frac{\cos^2(l)}{1 + (R_0/z_0)^2 \tan^2(b)}.$$

The projected intensity was fitted to the observed 2.2 μm DIRBE map (§ 2.1). The fitting method and error analysis are the same as those used for fitting triaxial models and are described in more detail in § 4.3 below.

The results of the fit are listed in Table 1 as model G0, and give a value of $R_0 = 0.91 \pm 0.01$ kpc; $z_0 = 0.51 \pm 0.01$ kpc, and $\rho_0 = (5.41 \pm 0.05) \times 10^7\ L_\odot\ \mathrm{pc}^{-3}$, with a reduced χ^2 value of 3.33 for about 3000 degrees of freedom. The z_0/R_0 axis ratio is 0.53, similar to the value of 0.61 derived by Kent et al. (1991) for their axisymmetric bulge model, and similar to the value of 0.6 derived by Weiland et al. (1994) for the ratio of the average projected 2.2 μm intensities in, respectively, the direction of the minor and major axes of the bulge. Maihara et al. (1978) derived a similar ratio of 0.52 from their analysis of the 2.4 μm data from the Galactic center region, while Matsumoto et al. (1982) derived a somewhat larger value of 0.75 from fitting their 2.4 and 3.4 μm data with a spheroidal source distribution.

The 2.2 μm intensity of the model in the direction of Baade's window is 9.3 MJy sr^{-1}, in general agreement with the observed value of $\sim$11 MJy sr^{-1}. The total 2.2 μm luminosity of the bulge in this model is $4.0 \times 10^8\ L_\odot$, in good agreement with the value of $4.1 \times 10^8\ L_\odot$ derived by a direct integration of the 2.2 μm DIRBE bulge map between $-10° \le l \le 10°$ and $-10° \le b \le 10°$ (see § 6.1). This value is within a factor of $\sim$1.5 of the luminosities derived for the other stellar distribution examined in this paper, and comparable to the value of $\sim 3.3 \times 10^8\ L_\odot$ derived by Kent (1992; note that the 2.4 μm bulge luminosity of $1.2 \times 10^{10}\ L_\odot$ quoted in Kent's paper is in units of the Sun's K-band luminosity). In spite of the relatively good agreement between this model and the data, if fails to account for the observed longitudinal asymmetry of the bulge. The asymmetry is apparent in the DIRBE data (Weiland et al. 1994), and in Figure 3*a*, which shows the systematic deviations of the data from the longitudinal symmetric model at positive Galactic longitudes. This leads us to examine various triaxial models for the bulge.

4.2. *Triaxial Bulge Models*

We have selected from the literature several functional forms, $\rho_{\mathrm{fun}}(x, y, z)$, previously chosen to fit the observed surface brightness profile of the Galactic bulge or bulges in external galaxies, to characterize the source distribution of the Galactic bulge. Some functions have been used to describe an axisymmetric source distribution, and their radial coordinate was modified (see eq. (4), to allow for a triaxial bulge morphology. The various functions considered for the density distribution of bulge sources fall into three categories which characterize their general behavior: *Gaussian-type functions* (*G*), which include: (a) a *Gaussian triaxial*, ρ_{G1}; (b) a "*boxy*" *Gaussian*, ρ_{G2}, with the special radial coordinate, r_s, representing a triaxial variation of the one used by Kent et al. (1991); and (c) a *Bahcall distribution*, ρ_{G3}. Originally suggested by Sanders & Lowinger (1972) as an axisymmetric $r^{-1.8}$ distribution, it was multiplied by a Gaussian function by Bahcall et al. (1982; see Bahcall 1986, for its functional presentation). The function was most recently used in its axisymmetric form by Wainscoat et al. (1992) to model the infrared point source morphology of the bulge; *exponential-type functions* (*E*) which include: (*d*) an *exponential triaxial*, ρ_{E1}. This functional form was used by Blitz & Spergel (1991) to characterize the bar morphology from the 2.4 μm observations of the Galactic center region by Matsumoto et al. (1982); (*e*) an *exponential triaxial*, ρ_{E2}, used by Whitelock & Catchpole (1992) to model the distribution of *IRAS* Mira variables in the bulge; and (*f*) a *modified spheroid*, ρ_{E3}. Kent et al. (1991) noted that the bulge component of the Galaxy is flattened along the poles, giving it a "boxy" appearance. They therefore adopted a density profile that is represented by a modified Bessel function K_0, and a special radial coordinate r_s (see eq. [4b]); and *power-law type functions* (*P*), which include: (*g*) a *power-law triaxial*, ρ_{P1}; (*h*) a *Hernquist profile*, ρ_{P2}. The motivation for this choice of density profile, summarized by Hernquist (1990), are that its projection on the sky resembles the de Vaucouleurs $R^{1/4}$ law at small radii (de

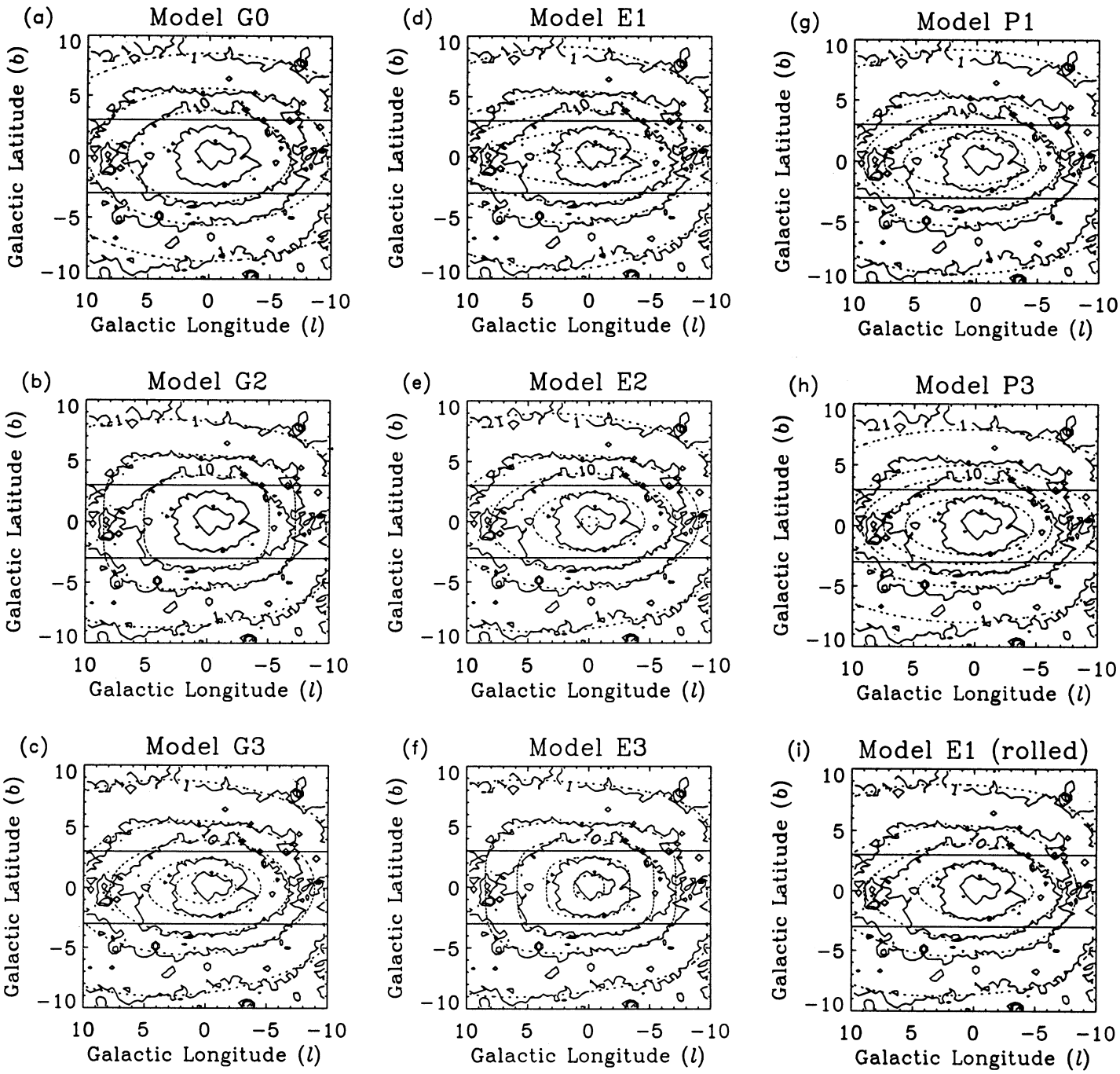

FIG. 3.—(*a*)–(*i*) Comparison of the DIRBE observations (*solid contours*) with the projected 2.2 μm intensity of selected models (*dotted contours*) calculated for $R_{CR} = 2.4$ kpc. The roll angle γ was held fixed at zero for the models in Figs. 3*a*–3*h*. Figure 3*i* depicts the effect of a roll on the functional form E1, shown with $\gamma = 0$ in Fig. 3*d*.

Vaucouleurs 1948), and that its potential is simply related to the density distribution ρ_{P2}; and finally, (*i*) a "*perfect*" *ellipsoid*, ρ_{P3}, used by de Zeeuw (1985) and Statler (1987) to model stellar orbits in elliptical galaxies. The following equations summarize the various functional forms used for ρ_{fun}, and the definition of their coordinate:

$$\rho_{G1}(x, y, z) = \rho_0 \exp(-0.5r^2), \quad (3a)$$

$$\rho_{G2}(x, y, z) = \rho_0 \exp(-0.5r_s^2), \quad (3b)$$

$$\rho_{G3}(x, y, z) = \rho_0 r^{-1.8} \exp(-r^3), \quad (3c)$$

$$\rho_{E1}(x, y, z) = \rho_0 \exp(-r_e), \quad (3d)$$

$$\rho_{E2}(x, y, z) = \rho_0 \exp(-r), \quad (3e)$$

$$\rho_{E3}(x, y, z) = \rho_0 K_0(r_s), \quad (3f)$$

$$\rho_{P1}(x, y, z) = \rho_0 \left(\frac{1}{1+r}\right)^4, \quad (3g)$$

$$\rho_{P2}(x, y, z) = \rho_0 \frac{1}{r(r+1)^3}, \quad (3h)$$

$$\rho_{P3}(x, y, z) = \rho_0 \left(\frac{1}{1+r^2}\right)^2, \quad (3i)$$

where $$r_e = \left[\left(\frac{|x|}{x_0}\right) + \left(\frac{|y|}{y_0}\right) + \left(\frac{|z|}{z_0}\right)\right], \quad (4a)$$

$$r = \left[\left(\frac{x}{x_0}\right)^2 + \left(\frac{y}{y_0}\right)^2 + \left(\frac{z}{z_0}\right)^2\right]^{1/2}, \quad (4b)$$

and $$r_s = \left\{\left[\left(\frac{x}{x_0}\right)^2 + \left(\frac{y}{y_0}\right)^2\right]^2 + \left(\frac{z}{z_0}\right)^4\right\}^{1/4}. \quad (4c)$$

The parameter ρ_0 in equations (3) is a normalization constant given in units of luminosity per unit volume and is determined from fitting the intensity $I(l, b)$ calculated from equation (1) to the observations. The various functional forms have quite different gradients at small and large galactocentric radii. Their projected intensities will therefore depend on their physical extent. On dynamical grounds, the stellar distribution functions cannot extend to galactocentric radii larger than the corotation radius, R_{CR}, beyond which stable stellar orbits cannot exist. This radius is about 2.4 ± 0.5 kpc (Binney et al. 1991). Weinberg (1992a) found observational evidence that the bar extends to ≈ 5 kpc from the Galactic center and appears to be circumscribed by the 5 kpc molecular ring. To show the dependence of the bar parameters on its physical extent, we performed the fits for three values of R_{max}, the cutoff radius in the Galactic plane: $R_{max} = \infty$, which means that each functional form was integrated until the line of sight intensity converged; $R_{max} = 5.0$ kpc to comply with the claimed observational constraint; and $R_{max} = 2.4$ kpc, to comply with the dynamical constraint. For numerical reasons, the cutoffs were implemented by multiplying the numerical functions by a function $f(r)$, given by

$$f(r) = 1.0 \quad \text{for } R_{xy} \equiv \sqrt{x^2 + y^2} < R_{max};$$
$$= \exp\left[-R_{xy}^2/2r_0^2\right] \quad \text{for } R_{xy} > R_{max}, \quad (5)$$
$$r_0 = 0.5 \text{ kpc}$$

which produced a smoothly varying transition to $\approx$zero for the source number density beyond R_{max}.

A bulge model is represented by a functional form, which is characterized by its axes x_0, y_0, and z_0; by its normalization constant ρ_0; and by its orientation, which is characterized by three rotation angles: the in-plane rotation α, out-of-plane tilt β, and out-of-plane roll γ. We determined the best-fitting model by a search for the minimum reduced χ^2 in the six-dimensional space spanned by these parameters (we initially ignored the roll and kept γ fixed at a value of 0) using an iterative least-squares minimization method known as the Marquardt-Levenberg algorithm (e.g., Press et al. 1986). Initial guesses were obtained by a crude search in parameter space, and the robustness of the minimization algorithm was confirmed by varying the parameters of the initial guesses. Parameter uncertainties were derived from the 68% joint confidence region of the parameters (Brand 1974; Eadie et al. 1971). The uncertainties derived by this method take into account the uncertainties in the data and the correlation among the parameters. All errors quoted in the parameters correspond to 1 σ deviations, i.e., to a 68% confidence level. The effect of a roll was investigated for only two models, keeping the tilt angle β fixed at zero. The results of the modeling efforts are discussed below.

5. BULGE MORPHOLOGY

5.1. *General Considerations and Comparison between the Functional Forms*

Table 1 presents the parameters and their 1 σ statistical uncertainties of the best-fitting models for the 2.2 μm intensity with $\gamma = 0$ (no roll), for each of the triaxial functional forms discussed above. Two values for χ_ν^2 are listed in the table. The first, labeled "fit," corresponds to the value of the reduced χ^2 for the region used to constrain the fit ($|l| \leq 10°$, $3° \leq |b| \leq 10°$); the second, labeled "tot," corresponds to the value of the reduced χ^2 for the entire bulge region ($|l| \leq 10°$, $|b| \leq 10°$), and is included in the table to assess the fit of the various functional forms to the lower latitude regions that were not used to constrain the fit. We emphasize that χ_ν^2(tot) is a measure of the agreement between an extrapolation of the model and the data in a region where we are uncertain of the extinction correction. It *does not* represent the minimum possible value that may be obtained when the fitting procedure includes the low-latitude data. In all cases, χ_ν^2 is calculated for about 3000 degrees of freedom. Both entries should only be used as a relative measure of the quality of each of the models. Since our uncertainties (σ) are non-Gaussian, and their values are somewhat uncertain, the resulting values of χ_ν^2 and χ_ν^2(tot) cannot be used to derive a rigorous estimate of a "goodness-of-fit," and hence to formally judge the relative merit of the various models, or the significance of the improvement in the fit between the models. Figure 3 compares the projected 2.2 μm intensity of selected models to the observations. The portions of the map for $|b| < 3°$ were not used in the fitting of the models, but are shown here to illustrate the behavior of the functions at small radii. Not surprisingly, considering the flattened appearance of the bulge, the best-fitting models (models G2 and E3, $\chi_\nu^2 \approx 2.1$) have intrinsically a "boxy" geometry which flattens the shape of the bulge both in the z direction and in the Galactic plane. Models which have "exponential" radial density distributions generally fit as well as the Gaussian functions ($\chi_\nu^2 \approx 2.1$–2.3), with the exception of model E1 which was somewhat worse ($\chi_\nu^2 \approx 2.7$). The "power-law" functions generally fit relatively poorly ($\chi_\nu^2 \geq 2.9$), since they have difficulty in fitting the outer portions of the bulge. The "power-law" functions are also more sensitive to the boundary condition, R_{max}, used in the modeling. Models P1 and P2 even failed to converge for certain conditions. We point out that there can be strong coupling between the parameters in Table 1. This is especially apparent in cases when the rotation angle $\alpha \rightarrow 90°$. Then large values of x_0 can be compensated for by small values of ρ_0. Model P1 at $R_{max} = 2.4$ kpc is the most extreme example of this coupling.

Tables 2 and 3, respectively, list results of the model fits to the 3.5 and 4.9 μm intensity of the bulge. Comparison of the tables show that the relative quality of the various functions remains the same, and the parameters of the models are similar. This occurs despite the lower extinction at these wavelengths, which allows extension of the modeled regions down to $|b| = 2°$. The results of these models therefore support the conclusions drawn from the 2.2 μm data. The similarity between the model results at these different wavelengths

TABLE 1

PARAMETERS OF THE BEST-FITTING TRIAXIAL MODELS AT 2.2 μm[a]

Model	R_{max} (kpc)	α	β	x_0 (kpc)	y_0 (kpc)	z_0 (kpc)	ρ_0 ($L_\odot$ kpc^{-3})	χ^2_ν Fit	χ^2_ν Total
G0.....	∞	0°.0	0°.0	0.91 ± 0.01		0.51 ± 0.01	(5.41 ± 0.054) × 10^7	3.33	
G1.....	2.4	73.8 ± 5.8	0.6 ± 0.3	3.11 ± 1.03	0.76 ± 0.03	0.48 ± 0.02	(3.05 ± 0.742) × 10^7	2.31	7.9
	5.0	79.2 ± 2.6	0.4 ± 0.2	2.12 ± 0.08	0.75 ± 0.01	0.45 ± 0.02	(3.25 ± 0.153) × 10^7	2.28	6.9
	∞	79.0 ± 2.4	0.4 ± 0.2	2.08 ± 0.06	0.75 ± 0.01	0.45 ± 0.02	(3.30 ± 0.151) × 10^7	2.28	
G2.....	2.4	70.7 ± 4.4	0.8 ± 0.4	1.56 ± 0.14	0.60 ± 0.02	0.45 ± 0.00	(3.85 ± 0.535) × 10^7	2.10	9.2
	5.0	76.6 ± 2.8	0.7 ± 0.3	1.58 ± 0.06	0.62 ± 0.01	0.43 ± 0.01	(3.66 ± 0.184) × 10^7	2.06	8.2
	∞	76.6 ± 2.8	0.7 ± 0.3	1.58 ± 0.05	0.62 ± 0.01	0.43 ± 0.01	(3.66 ± 0.180) × 10^7	2.06	
G3.....	2.4	59.0 ± 9.5	0.7 ± 0.4	3.78 ± 0.25	1.44 ± 0.17	1.19 ± 0.02	(9.06 ± 2.80) × 10^6	2.28	9.7
	5.0	69.9 ± 6.7	0.7 ± 0.3	4.03 ± 0.14	1.67 ± 0.05	1.12 ± 0.03	(7.42 ± 0.86) × 10^6	2.28	11.0
	∞	69.7 ± 6.8	0.7 ± 0.3	4.01 ± 0.14	1.67 ± 0.05	1.12 ± 0.03	(7.42 ± 0.86) × 10^6	2.28	
E1	2.4	65.7 ± 4.6	0.5 ± 0.3	2.23 ± 0.19	0.65 ± 0.07	0.32 ± 0.01	(2.21 ± 0.462) × 10^8	2.65	17.2
	5.0	67.9 ± 6.5	0.4 ± 0.3	1.67 ± 0.05	0.65 ± 0.10	0.31 ± 0.01	(2.47 ± 0.399) × 10^8	2.71	18.9
	∞	65.6 ± 6.7	0.5 ± 0.3	1.64 ± 0.06	0.61 ± 0.11	0.31 ± 0.01	(2.64 ± 0.437) × 10^8	2.72	
E2	2.4	49.0 ± 8.8	0.6 ± 0.4	0.75 ± 0.05	0.19 ± 0.33	0.27 ± 0.01	(5.18 ± 5.82) × 10^8	2.30	5.1
	5.0	48.7 ± 13.5	0.6 ± 0.4	0.74 ± 0.06	0.16 ± 0.57	0.27 ± 0.02	(6.04 ± 12.4) × 10^8	2.30	4.9
	∞	48.7 ± 13.5	0.6 ± 0.4	0.74 ± 0.06	0.16 ± 0.57	0.27 ± 0.02	(6.04 ± 12.4) × 10^8	2.30	
E3	2.4	49.8 ± 9.4	0.7 ± 0.4	0.69 ± 0.05	0.19 ± 0.27	0.28 ± 0.01	(4.58 ± 4.21) × 10^8	2.12	4.0
	5.0	51.0 ± 13.3	0.7 ± 0.4	0.69 ± 0.06	0.19 ± 0.33	0.28 ± 0.01	(4.59 ± 5.20) × 10^8	2.12	4.0
	∞	51.4 ± 13.7	0.7 ± 0.4	0.70 ± 0.06	0.20 ± 0.32	0.28 ± 0.01	(4.45 ± 4.38) × 10^8	2.12	
P1	2.4	81.6 ± 1.0	0.3 ± 0.2	3.1E5 ± 0	0.60 ± 0.04	0.33 ± 0.03	(6.10 ± 1.13) × 10^8	3.04	93.7
	5.0	...	...	...	...	...	...	...	
	∞	53.6 ± 2.6	0.6 ± 0.4	0.41 ± 0.10	0.14 ± 0.10	0.14 ± 0.05	(3.32 ± 2.87) × 10^{10}	2.61	
P2	2.4	...	...	...	...	...	...	...	
	5.0	88.5 ± 0.3	0.1 ± 0.0	8.81 ± 4.21	0.45 ± 0.35	0.24 ± 0.25	(2.68 ± 6.76) × 10^8	3.06	254.1
	∞	55.4 ± 17.5	0.6 ± 0.4	0.63 ± 0.22	0.19 ± 0.39	0.19 ± 0.06	(7.70 ± 14.9) × 10^9	2.97	
P3	2.4	85.8 ± 0.2	0.2 ± 0.2	10.4 ± 40.3	0.60 ± 0.36	0.28 ± 0.24	(2.71 ± 7.08) × 10^8	3.96	153.7
	5.0	88.4 ± 0.4	0.1 ± 0.0	6.25 ± 2.1	0.43 ± 0.13	0.23 ± 0.10	(1.62 ± 2.10) × 10^8	2.90	48.5
	∞	54.6 ± 33.3	0.5 ± 0.4	0.90 ± 0.2	0.23 ± 0.98	0.28 ± 0.04	(1.46 ± 4.49) × 10^9	2.85	

[a] The roll angle has been kept constant at a value of $\gamma = 0$. The reduced χ^2 was calculated for the fitted (χ^2_ν fit) and total (χ^2_ν tot) region of the bulge (see § 5.1 for details).

TABLE 2

PARAMETERS OF THE BEST-FITTING TRIAXIAL MODELS AT 3.5 μm[a]

Model	R_{max} (kpc)	α	β	x_0 (kpc)	y_0 (kpc)	z_0 (kpc)	ρ_0 ($L_\odot$ kpc^{-3})	χ^2_ν Fit	χ^2_ν Total
G1.....	2.4	75°.3 ± 4°.2	0°.9 ± 0°.3	2.64 ± 0.56	0.72 ± 0.01	0.48 ± 0.01	(1.73 ± 0.334) × 10^7	1.86	4.4
	5.0	82.1 ± 1.3	0.6 ± 0.2	2.30 ± 0.06	0.70 ± 0.01	0.44 ± 0.01	(1.67 ± 0.62) × 10^7	1.76	3.8
G2.....	2.4	76.5 ± 2.1	1.0 ± 0.3	2.01 ± 0.19	0.62 ± 0.01	0.44 ± 0.00	(1.83 ± 0.18) × 10^7	1.62	4.6
	5.0	79.9 ± 1.4	0.8 ± 0.2	1.72 ± 0.04	0.62 ± 0.01	0.41 ± 0.01	(1.91 ± 0.07) × 10^7	1.54	4.3
G3.....	2.4	53.2 ± 8.7	0.9 ± 0.4	3.41 ± 0.15	1.18 ± 0.28	1.25 ± 0.02	(5.66 ± 2.48) × 10^6	1.77	3.5
	5.0	68.2 ± 5.6	1.0 ± 0.3	3.94 ± 0.11	1.61 ± 0.06	1.18 ± 0.02	(3.72 ± 0.47) × 10^6	1.77	4.0
E1	2.4	65.5 ± 3.9	0.7 ± 0.4	2.00 ± 0.13	0.58 ± 0.06	0.35 ± 0.01	(1.07 ± 0.19) × 10^8	2.34	5.1
	5.0	68.2 ± 4.9	0.7 ± 0.3	1.64 ± 0.05	0.58 ± 0.08	0.34 ± 0.01	(1.12 ± 0.17) × 10^8	2.37	5.1
E2	2.4	47.3 ± 10.8	0.7 ± 0.4	0.74 ± 0.03	0.12 ± 0.80	0.28 ± 0.01	(3.67 ± 12.0) × 10^8	1.72	3.2
	5.0	47.8 ± 11.6	0.7 ± 0.4	0.74 ± 0.05	0.13 ± 0.70	0.28 ± 0.01	(3.37 ± 9.35) × 10^8	1.72	3.1
E3	2.4	49.1 ± 6.1	0.7 ± 0.4	0.73 ± 0.03	0.17 ± 0.29	0.29 ± 0.00	(2.38 ± 2.41) × 10^8	1.64	3.0
	5.0	50.1 ± 9.9	0.7 ± 0.4	0.74 ± 0.05	0.16 ± 0.37	0.29 ± 0.01	(2.51 ± 0.35) × 10^8	1.62	3.0
P1	2.4	75.4 ± 4.0	0.9 ± 0.4	2.02 ± 0.47	0.54 ± 0.10	0.34 ± 0.06	(3.95 ± 2.31) × 10^8	2.55	5.6
	5.0	88.4 ± 0.4	0.1 ± 0.1	6.62 ± 1.79	0.43 ± 0.12	0.34 ± 0.09	(2.30 ± 2.20) × 10^8	2.79	11.5
P2	2.4	86.6 ± 7.3	0.1 ± 0.6	2.48 ± 3.88	0.74 ± 0.81	0.34 ± 0.53	(1.45 ± 6.87) × 10^8	4.81	21.6
	5.0	88.1 ± 0.5	0.2 ± 0.1	5.76 ± 1.15	0.55 ± 0.14	0.30 ± 0.10	(9.31 ± 9.31) × 10^7	2.84	28.4
P3	2.4	74.2 ± 4.5	0.9 ± 0.3	2.62 ± 0.41	0.73 ± 0.07	0.48 ± 0.03	(5.16 ± 1.80) × 10^7	2.23	3.7
	5.0	88.1 ± 0.4	0.2 ± 0.1	6.81 ± 0.88	0.56 ± 0.02	0.31 ± 0.02	(3.79 ± 1.25) × 10^7	2.55	5.6

[a] The roll angle has been kept constant at a value of $\gamma = 0$. The reduced χ^2 was calculated for the fitted (χ^2_ν fit) and total (χ^2_ν tot) region of the bulge (see § 5.1 for details).

TABLE 3

PARAMETERS OF THE BEST-FITTING TRIAXIAL MODELS AT 4.9 μm[a]

Model	R_{max} (kpc)	α	β	x_0 (kpc)	y_0 (kpc)	z_0 (kpc)	ρ_0 ($L_\odot$ kpc^{-3})	χ^2_ν Fit	χ^2_ν Total
G1.....	2.4	76°.8 ± 3°.4	1°.8 ± 0°.4	3.12 ± 0.75	0.76 ± 0.01	0.50 ± 0.01	(2.91 ± 0.50) × 10^6	1.81	4.2
	5.0	83.0 ± 1.3	1.0 ± 0.2	2.38 ± 0.07	0.71 ± 0.01	0.45 ± 0.01	(2.91 ± 0.19) × 10^6	1.73	3.8
G2.....	2.4	79.4 ± 1.4	1.5 ± 0.3	2.82 ± 0.32	0.64 ± 0.01	0.46 ± 0.00	(2.88 ± 0.21) × 10^6	1.62	4.2
	5.0	81.1 ± 1.4	1.3 ± 0.3	1.78 ± 0.04	0.63 ± 0.01	0.42 ± 0.01	(3.31 ± 0.13) × 10^6	1.58	4.1
G3.....	2.4	63.0 ± 6.4	1.8 ± 0.5	4.01 ± 0.22	1.59 ± 0.09	1.27 ± 0.01	(6.94 ± 1.38) × 10^5	1.82	3.6
	5.0	76.1 ± 3.2	1.7 ± 0.4	4.50 ± 0.11	1.76 ± 0.03	1.17 ± 0.02	(5.53 ± 0.32) × 10^5	1.78	3.7
E1	2.4	68.8 ± 3.8	1.6 ± 0.3	2.17 ± 0.20	0.66 ± 0.05	0.36 ± 0.01	(1.63 ± 0.29) × 10^7	2.33	4.8
	5.0	75.3 ± 3.3	1.4 ± 0.3	1.67 ± 0.05	0.72 ± 0.03	0.35 ± 0.01	(1.58 ± 0.14) × 10^7	2.24	4.7
E2	2.4	47.2 ± 11.5	1.3 ± 0.5	0.74 ± 0.06	0.14 ± 0.73	0.29 ± 0.01	(1.45 ± 4.12) × 10^8	1.72	3.5
	5.0	47.9 ± 12.6	1.3 ± 0.5	0.75 ± 0.06	0.15 ± 0.64	0.29 ± 0.01	(1.33 ± 3.19) × 10^8	1.72	3.5
E3	2.4	45.7 ± 2.3	0.8 ± 0.5	0.72 ± 0.03	0.08 ± 0.54	0.31 ± 0.00	(9.27 ± 24.9) × 10^7	1.69	3.2
	5.0	46.2 ± 13.0	0.8 ± 0.5	0.72 ± 0.06	0.08 ± 1.65	0.31 ± 0.01	(9.39 ± 78.6) × 10^7	1.69	3.2
P1	2.4	77.6 ± 3.0	2.4 ± 0.5	2.14 ± 0.44	0.61 ± 0.09	0.38 ± 0.06	(5.88 ± 2.97) × 10^7	2.30	4.8
	5.0	88.4 ± 0.4	0.4 ± 0.1	6.48 ± 1.44	0.47 ± 0.10	0.26 ± 0.08	(3.63 ± 2.85) × 10^7	2.45	7.5
P2	2.4	72.1 ± 5.2	2.1 ± 0.5	2.20 ± 0.39	0.74 ± 0.13	0.50 ± 0.07	(2.10 ± 1.26) × 10^7	2.36	7.9
	5.0	87.9 ± 0.5	0.5 ± 0.1	5.13 ± 0.87	0.56 ± 0.11	0.32 ± 0.08	(1.70 ± 1.38) × 10^7	2.51	17.5
P3	2.4	78.4 ± 3.0	2.1 ± 0.4	3.60 ± 0.63	0.84 ± 0.06	0.53 ± 0.03	(6.68 ± 2.00) × 10^6	2.05	3.8
	5.0	75.3 ± 4.0	2.0 ± 0.4	1.79 ± 0.11	0.62 ± 0.02	0.41 ± 0.01	(1.38 ± 1.87) × 10^7	2.30	3.9

[a] The roll angle has been kept constant at a value of $\gamma = 0$. The reduced χ^2 was calculated for the fitted (χ^2_ν fit) and total (χ^2_ν tot) region of the bulge (see § 5.1 for details).

should not be too surprising given the strong similarity of the bulge in all the extinction-corrected near-IR bands as seen in Figure 1.

Slices of the intensity distribution of models and observations at $l = 0°$ are shown in Figures 4*a*–4*c*. In the high-latitude regions used to constrain the fits, the differences between the functional forms are apparent as differences in the change of the intensity gradient with latitude. More obvious differences are found in the inner regions which were not constrained by our fitting procedure. The Gaussian functions (with the exception of G3, which is actually a hybrid function with a Gaussian-like outer portion and a power-law core) have very flat tops in contrast to the sharp peaks exhibited by power-law functions. Keeping in mind that the low-latitude data may be unreliable because of the extinction corrections in the inner portions of the bulge, the value of χ^2_ν(tot) suggests that the functions E2 and E3 provide the best overall fit to the data. However, the $l = 0$ slices (see Fig. 4) suggest that the function G3 seems to provide a better fit to the inner $|b| \leq 1/2°$ region of the bulge. The DIRBE trend, as displayed by function G3, represents therefore a continuation of the $r^{-1.8}$ behavior of the 2.2 μm intensity, first observed in a 15′ radius around the Galactic center (Becklin & Neugebauer 1968), to a radius of a few degrees. A similar large-scale behavior was observed by Matsumoto et al. (1982). The qualitatively different behavior of the various functional forms at low Galactic latitudes is also manifested in the differences between their χ^2_ν(tot) values. When the quality of the fit in these regions is taken into account, the χ^2_ν(tot) of the power-law function becomes significantly larger than the best-fitting functions. A similar effect, but somewhat reduced in magnitude, is seen for the function E1.

5.2. *Bulge Axis Ratios*

The scale lengths and densities have different meanings for the different functional forms and therefore cannot be directly compared to each other. However, functions G3, E1, E2, and E3 were previously used to fit either the projected intensity or stellar distribution of the bulge, and can be compared to the values derived in this paper (see Table 1). The axial parameters $\{x_0:y_0:z_0\}$ derived for these models are (in units of kpc): $\{2.0:2.0:1.58\}$ for an oblate spheroidal version of G3 fitted to the *IRAS* 12 and 25 μm IR sky (Wainscoat et al. 1992); $\{1.0:0.7:0.7\}$ for E1, the function used by Blitz & Spergel (1991) to model the Matsumoto et al. (1982) 2.4 μm photometry; $\{0.71:0.18:0.18\}$ for E2 fitted to the distribution of bulge Mira variables (Whitelock & Catchpole 1992); and $\{0.67 \pm 0.23:0.67 \pm 0.23:0.41 \pm 0.14\}$ for an oblate spheroidal version of E3 fitted to the 2.4 μm IRT data (Kent et al. 1991). The comparison with the results obtained by Whitelock & Catchpole is especially interesting, since it provides a measure of the differences in the spatial distribution of the bulge Miras and the 2.2 μm emission sources (K and M giants). The results show that the most significant difference in the distribution of these two stellar populations is their scale height. Based on our model E2 results, the K and M giants have typical vertical scale lengths of ~270 pc, whereas the Mira distribution is significantly flatter with a scale length of $z_0 \approx 180$ pc. The models show no significant differences in their scale lengths along the other axes. The difference in the morphology of these two populations may seem puzzling considering the widely held view that M stars evolve into Miras. However, Whitelock (1993) discussed the possible reasons for this morphological difference. The *IRAS* Miras were selected on the basis of their *IRAS* fluxes, and therefore represent Miras with particularly high mass-loss rates. They will have either more massive (or younger) or more metal-rich progenitors than "typical" Miras, which can explain their increased concentration toward the Galactic center. Furthermore, the selected Miras do not represent a spatially well-sampled population, so that any inferences on their vertical scale height is currently premature.

A quantity that can be compared between the different functional forms is the ratio of various axes. Figure 5 depicts the

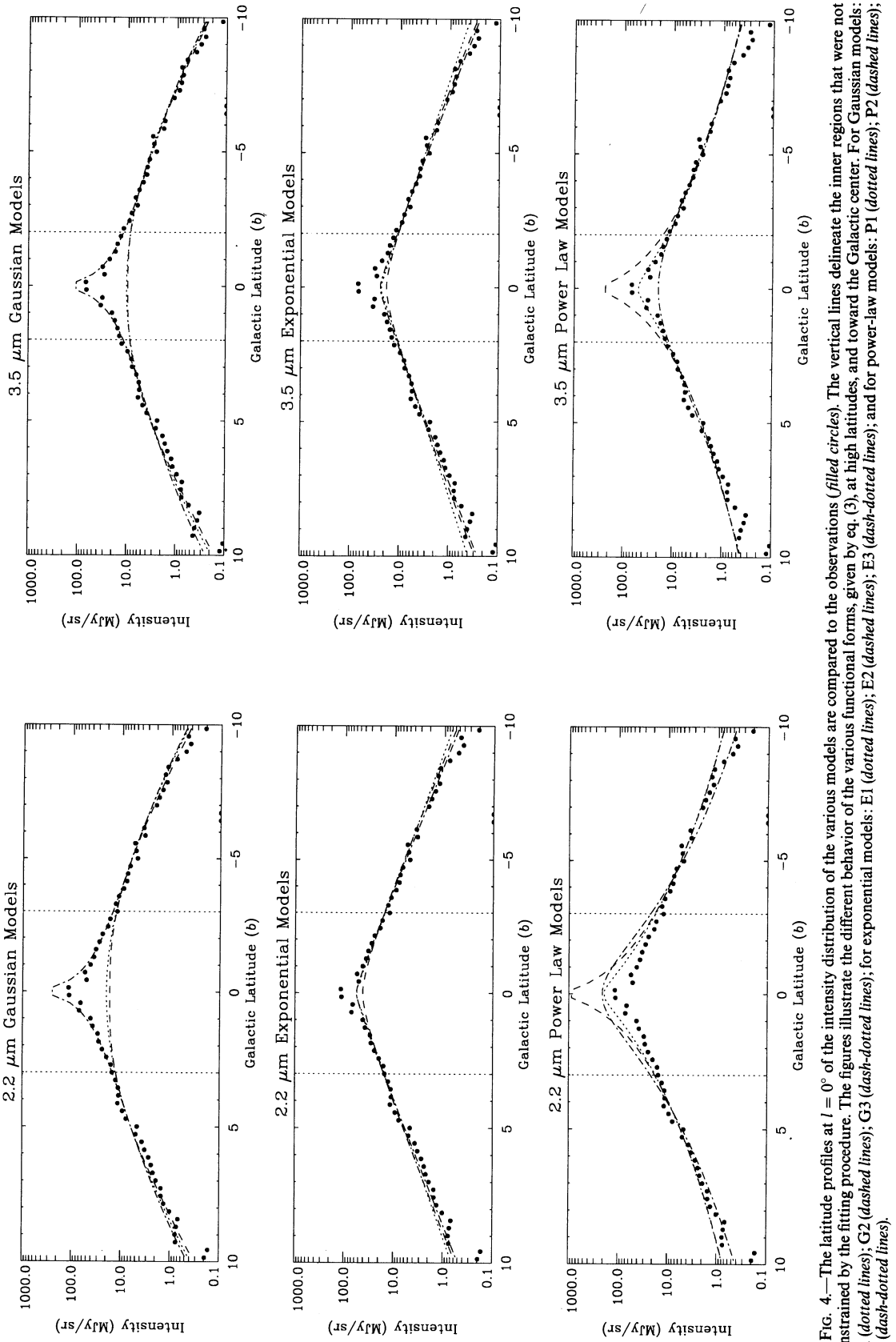

FIG. 4.—The latitude profiles at $l = 0°$ of the intensity distribution of the various models are compared to the observations (*filled circles*). The vertical lines delineate the inner regions that were not constrained by the fitting procedure. The figures illustrate the different behavior of the various functional forms, given by eq. (3), at high latitudes, and toward the Galactic center. For Gaussian models: G1 (*dotted lines*); G2 (*dashed lines*); G3 (*dash-dotted lines*); for exponential models: E1 (*dotted lines*); E2 (*dashed lines*); E3 (*dash-dotted lines*); for power-law models: P1 (*dotted lines*); P2 (*dashed lines*); P3 (*dash-dotted lines*).

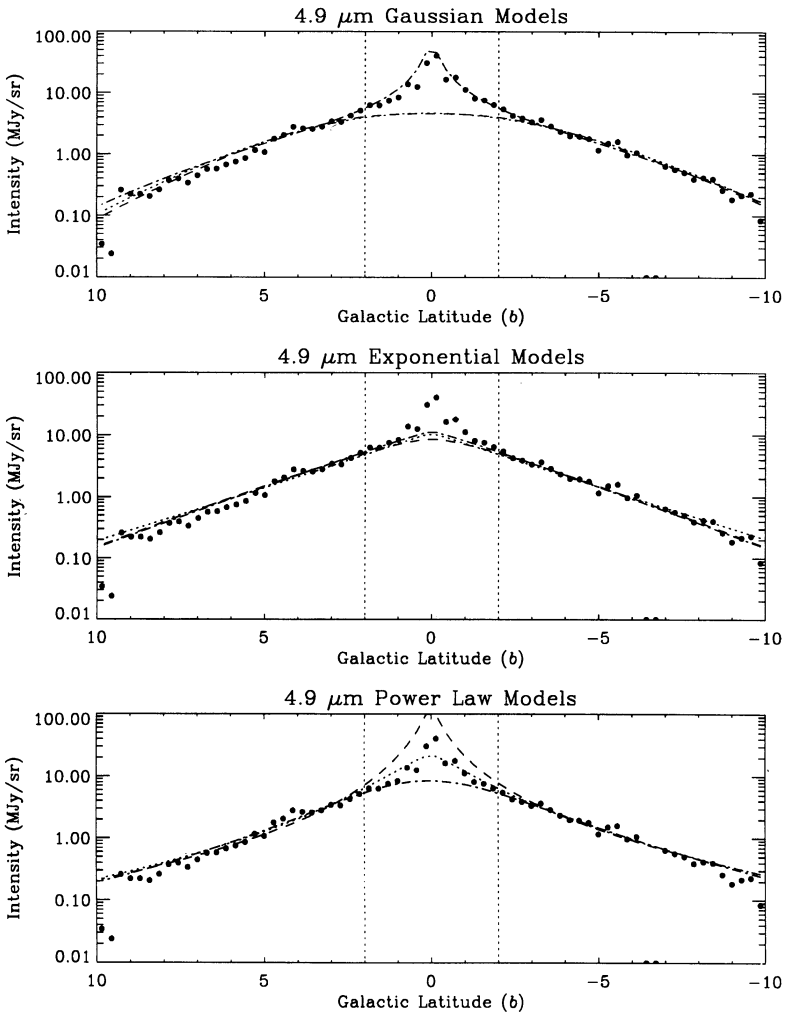

FIG. 4—*Continued*

x_0/y_0 and z_0/y_0 axis ratios of the various models for the 2.2, 3.5, and 4.9 μm observations. The horizontal scatter of the data was done for the sake of clarity in the presentation. The results show that regardless of the functional form and the wavelength of the observations, $x_0/y_0 \approx 3 \pm 1$, $z_0/y_0 \approx 0.7 \pm 0.3$, $z_0/(x_0^2 + y_0^2)^{1/2} = 0.74 \pm 0.4$. The latter ratio is somewhat larger than that derived for an axisymmetric bulge model (§ 4.1) or from the observed drop-off in the projected intensities along the x and z-axes of the bulge (Weiland et al. 1994). The average axis ratios derived here translate to axial ratios of $\{x_0:y_0:z_0\} = \{1:0.33 \pm 0.11:0.23 \pm 0.8\}$. In particular, model G3 gives axial ratios of $\{1:0.38 \pm 0.05:0.33 \pm 0.03\}$, whereas Vietri (1986) derived axial ratios of $\{1:0.7:0.4\}$ for the same functional form. Another quantity of interest is the bulge triaxiality, defined here as the ratio

$$\mathcal{T} \equiv \frac{1 - (y_0/x_0)^2}{1 - (z_0/x_0)^2} .$$

Note that $\mathcal{T}$ is equal to 0 and 1 for oblate and prolate spheroids, respectively. The triaxiality of the bulge is in the range: $\mathcal{T} \approx 0.81$–0.94, close to that of a prolate spheroid.

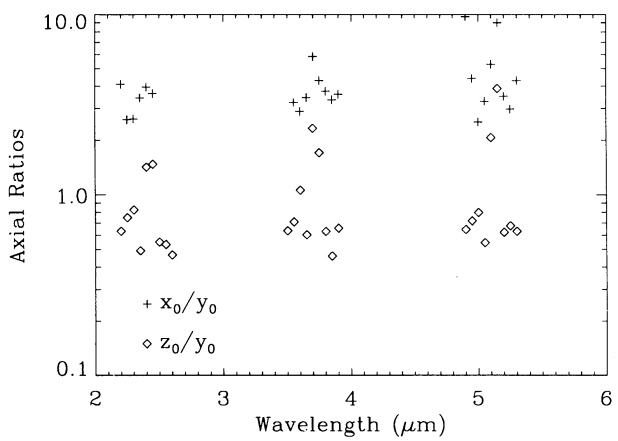

FIG. 5.—The axis ratios x_0/y_0 and z_0/y_0 for the various models at 2.2, 3.5, and 4.9 μm. The horizontal spread along the x-axis in each band was done for sake of clarity.

5.3. *Bulge Orientation*

The rotation and tilt angles (α, β) are defined in the same way for each model and also allow for a direct comparison between the various models. The best-fitting models G2 and E3 give values of $\alpha \approx 74°$ and 50°, respectively. The rotation angles of

all models lie in the range $\alpha \approx 50°$–$90°$, with an average of $\alpha \approx 65°$ if the power-law functions are excluded, and with a $\pm 15°$ uncertainty reflecting the variance of the different models. Binney et al. (1991) have argued from studies of the kinematics of the H I, CO, and CS gas in the central region of the Galaxy that the flow of the gas is dominated by a bar which should have a viewing angle of $16° \pm 2°$. Weinberg (1992a), on the other hand, suggested a viewing angle of $36° \pm 10°$ for the bar. These "viewing" angles correspond to values of $\alpha = 74° \pm 2°$ and $\alpha = 54° \pm 10°$, respectively, in our notation (see Fig. 2). The Binney et al. kinematic model therefore favors the Gaussian-type function G2 which has $\alpha = 70.^\circ7 \pm 4.^\circ4$, over the functional form E3 that was used by Kent et al. which gives $\alpha = 49.^\circ8 \pm 9.^\circ4$. Weinberg's model, however, favors the modified Bahcall & Soneira function, G3, which has a value of $\alpha = 59.^\circ0 \pm 9.^\circ5$.

From an observed tilt in the streamlines of the H I and CO gas located within 2 kpc of the Galactic center, Liszt & Burton (1980) argued that the bulge should be tilted out of the Galactic plane as well. The data allow for an out-of-plane tilt of the bulge; however, at 2.2 μm the tilt angles β of the various models are small, typically $\approx 0.^\circ6$, and are never larger than 3 σ from zero. Results from 3.5 and 4.9 μm suggest that the tilt may be increasing with wavelength; however, β is always $\leq 2°$. Such small tilt angles could be caused by a nonuniform distribution of foreground stars. Our conclusion is therefore consistent with that reached by Weiland et al. (1994), who found no evidence for a tilt in the data. Blitz & Spergel argued from the Matsumoto et al. data that the bar should be tilted by as much as 7°. Tilting any of the models by $\beta = 7°$ will produce a longitudinal difference map that is inconsistent with the DIRBE data. The difference between our result and that of Blitz & Spergel can probably be attributed to the improved data used in the current modeling effort, especially the improved correction for interstellar extinction.

5.4. *The Effect of a Roll*

We have examined the effect of a roll ($\gamma \neq 0$), initially suppressing any tilt of the bulge (i.e., β was kept equal to zero), on two functional forms: the Blitz-Spergel function (E1), and the boxy Gaussian (G2). We have chosen to study the effect of the roll on function E1 because, of all the nonpower-law functions it provided the worst fit to the data, and had a distinctly non-"boxy" appearance (see Fig. 3*d*). Model G2 was chosen since it provided the best fit to the data, and we want to see whether a roll could provide a better fit to the data. Model parameters that provided the best fit of these functions to the 2.2 μm intensity are listed in Table 4. The roll had a minor effect on the quality of the fit of the function G2, and actually worsened the fit to the data. The effect of the roll was most dramatic for the function E1, which is shown in Figure 3*i*. By rolling the function by $\sim 45°$ the projected intensity attained an almost "boxy" character, distinctly different from the elongated appearance it had in Figure 3*d*. The effect of the roll on E1 is peculiar to that function because of its definition of the radial coordinate r_e (see eq. [4a]). Surfaces of constant r_e are octahedral, and a roll of $\sim 45°$ about the major axis can produce a "boxy" projection.

Similar results for these models were obtained for cases in which all three angles were allowed to vary simultaneously. Again, the 45° roll preferred by model E1 represents the peculiar definition of r_e, rather than an intrinsic roll of the Galactic bulge.

6. LUMINOSITY AND LUMINOUS MASS

6.1. *The Observed In-Band Luminosities*

The observed luminosity in the various DIRBE bands can be obtained by integrating the maps over the $|l| \leq 10°$, and $|b| \leq 10°$ region (area of 0.122 sr). Assuming a distance of 8.5 kpc to the Galactic center, the bulge luminosities in the 2.2, 3.5, and 4.9 μm DIRBE bands, with corresponding bandwidths of 2.28×10^{13}, 2.10×10^{13}, and 8.61×10^{12} Hz, are 4.1×10^8, 2.3×10^8, and 4.3×10^7 $L_\odot$, respectively. The 1.25 μm intensity map of the bulge differs from that at 2.2 μm by a simple scaling factor of 2.9, giving a 1.25 μm luminosity of 1.2×10^9 $L_\odot$. The main uncertainty in the observed luminosities is the low-latitudes ($|l| \leq 3°$) extinction, especially at the shorter wavelengths. However, the similarity between the 4.9 and 2.2 μm maps suggest that the effect may not be too large. To estimate the magnitude of this effect we varied the 2.2 μm optical depth by factors of 0.5 and 2 from its nominal value over the entire bulge region. As a result the luminosity in this band varied by factors of 0.8 and 1.8, respectively. At 4.9 μm, the same variations in the optical depth changed the luminosity by factors of 0.95 and 1.1, respectively.

The luminosities derived from the intensities and the assumed source distance of 8.5 kpc do not take the three-dimensional structure of the bulge into account. This is done by integrating the in-band volume emissivity of the various models. At 2.2 μm (K band) this volume integral is given by

$$L_{K;\,\mathrm{bulge}} = \int_V \rho_s \, dV \,, \tag{6}$$

where ρ_s is the 2.2 μm volume emissivity of the sources determined from fitting the model to the DIRBE observations. The parameters for ρ_s(2.2 μm) for the various functional forms are given in Table 1. The volume integral was done numerically, and its accuracy was checked for the functions which have an analytical expression for the volume integral in the $R_{\max} \rightarrow \infty$ limit. Table 5 gives the resulting luminosity of the bar in the 2.2, 3.5, and 4.9 μm DIRBE bands for $R_{\max} = 2.4$ kpc.

The main sources of uncertainty in the luminosities derived in the models arise due to the uncertainties in the model

TABLE 4

PARAMETERS OF THE BEST-FITTING TRIAXIAL MODELS AT 2.2 μm[a]

Model	$R_{\max}$ (kpc)	α	γ	x_0 (kpc)	y_0 (kpc)	z_0 (kpc)	ρ_0 ($L_\odot$ kpc^{-3})	χ^2_ν Fit	χ^2_ν Total
E1	2.4	$59.^\circ4 \pm 2.^\circ0$	$45.^\circ0 \pm 2.^\circ9$	1.61 ± 0.06	0.37 ± 0.01	0.36 ± 0.01	$(3.05 \pm 0.28) \times 10^8$	2.36	5.3
G2.....	2.4	68.5 ± 4.8	90.7 ± 1.5	2.03 ± 0.23	0.47 ± 0.01	0.58 ± 0.02	$(3.54 \pm 0.51) \times 10^7$	2.31	8.5

[a] The tilt angle has been kept constant at a value of $\beta = 0$. The reduced χ^2 was calculated for the fitted (χ^2_ν fit) and total (χ^2_ν tot) region of the bulge (see § 5.1 for details).

TABLE 5

BULGE LUMINOSITIES IN THE VARIOUS DIRBE BANDS[a]

Functional Form[b]	$L(2.2\ \mu m)$ $(L_\odot)$	$L(3.5\ \mu m)$ $(L_\odot)$	$L(4.9\ \mu m)$ $(L_\odot)$
G1	3.5×10^8	1.8×10^8	3.5×10^7
G2	3.1×10^8	1.7×10^8	3.3×10^7
G3	5.5×10^8	2.5×10^8	4.9×10^7
E1	5.8×10^8	2.6×10^8	4.8×10^7
E2	4.5×10^8	2.1×10^8	9.8×10^7
E3	4.0×10^8	2.0×10^8	3.9×10^7
P1	6.9×10^8	2.5×10^8	4.8×10^7
P2	6.0×10^8 [c]	2.8×10^8	5.7×10^7
P3	7.9×10^8	2.3×10^8	4.2×10^7
Observations[d]	4.1×10^8	2.3×10^8	4.3×10^7

[a] All luminosities were calculated for a Galactocentric distance of 8.5 kpc, and $R_{max} = 2.4$ kpc. The 1.25 μm luminosity for the various models can be obtained by multiplying the corresponding 2.2 μm entries by a factor of 2.9.

[b] The definition of the functional forms are given in eq. (3).

[c] Calculated for $R_{max} = 5.0$ kpc.

[d] The observational values were obtained by integrating the extinction-corrected, zodi- and disk-subtracted maps over the $|l| \leq 10°$ and $|b| \leq 10°$ region area around the Galactic center.

parameters, and due to the extrapolation of the volume emissivity function to the low-latitude regions that were not included in the fitting procedure. The Gaussian functions generally underestimate the central brightness, while the power-law functions tend to overestimate this value (see Figs. 4*a*–4*c*). An additional source of error is introduced by the uncertainties in the low-latitude extinction correction, which has the largest effect on the shortest wavelengths. The uncertainties in the luminosities due to the model parameters is primarily determined by the uncertainties in ρ_0, x_0, and z_0 (y_0 and ρ_0 are highly correlated), with ρ_0 the dominant source of uncertainty. Combined with our uncertainty estimates for the 2.2 μm extinction, average uncertainties in the luminosities are $\sim \pm 30\%$ for the Gaussian models, and factors of ~ 2 and ~ 3 for the exponential and power-law functions, respectively. For the sake of definiteness, we will adopt a nominal value of $4.0 \times 10^8\ L_\odot$ for the 2.2 μm luminosity of the bulge with an uncertainty of $\pm 1.2 \times 10^8\ L_\odot$.

Analysis of the near-infrared DIRBE data from the Galactic center region shows that the emission is dominated by that of K and M giant stars (Arendt et al. 1994). This confirms previous observations that K–M giants are the main contributors to the *K*-band luminosity from Baade's window (Frogel, Whitford, & Rich 1984; Frogel & Whitford 1987). The total bolometric luminosity of the bulge can then be estimated from the 2.2 μm luminosity by adopting a typical star to represent the spectrum of the bulge stellar population, and making the appropriate bolometric correction. Taking an M0 giant with an effective temperature of 3800 K to represent the spectrum of a typical bulge giant yields a bolometric correction to the 2.2 μm luminosity of ~ 14.5, and a bolometric luminosity of $5.8 \times 10^9\ L_\odot$.

6.2. *The K-Band Luminosity Function of the Bulge*

The bolometric luminosity of the bulge was derived by adopting a "typical" spectral type giant to represent the bulge population. The choice of spectral type affects not only the derived bolometric luminosity, but the inferred number of K and M giants as well. The bolometric luminosities of these stars increases by more than two orders of magnitude from spectral type K0 to M9, whereas their masses are comparable. Consequently, the number of bulge giants and the photometrically derived bulge mass depend rather sensitively on the choice of representative spectral type. The bolometric luminosity of the bulge can be derived more accurately by utilizing the results of extensive ground-based *K*-band (2.2 μm) observations of the bulge K and M giant population in the direction of Baade's window. From these observations, previous studies provide a *K*-band luminosity function (LF) which, renormalized to fit the DIRBE-determined 2.2 μm bulge luminosity, can be adopted for the bulge as a whole.

Frogel & Whitford (1987, hereafter FW) were the first to derive the LF for an unbiased subsample of spectroscopically selected M1–9 giants in Baade's window ($l = 1°$; $b = -3.9°$) with magnitudes of $K \approx 6$–10. A deeper survey, not restricted to M giants, was conducted by DePoy et al. (1993, hereafter DP). Their *K*-band luminosity function shows that after the FW luminosity function is scaled up by a factor of 1.29 to take account of the difference in the areas of the surveyed fields, the two luminosity functions are in very good agreement for magnitudes between $K \approx 9$–10. This agreement suggests that M giants account for more than 90% of the 2.2 μm flux. The results of the FW survey and the fainter DP survey can therefore be combined to construct the *K*-band LF of the stars in a 604 arcmin^2 area of Baade's window over the entire ~ 7 to ~ 13 magnitude range. Defining $\Phi_{BW}(K)dK$ to be the number of stars with magnitudes in the $K - K + dK$ interval, a fit to the data presented in Figure 3 of DePoy et al. (1993) gives

$$\Phi_{BW}(K) = 0.907 \times 10^{0.3045K} \text{ stars mag}^{-1} \quad \text{for } 6.8 < K < 13.3 . \quad (7)$$

The magnitude limits of the LF were determined by the observed fall off in the LF for bright stars in the FW survey, and incompleteness in the counts at the faint end due to crowding effects in the DP survey. At the faint end we could have, in principle, adopted the LF of Davidge (1991) which extended the survey depth to $K \approx 16$ mag. However, we chose to cut off the faint end of the LF at a magnitude of 13.3 since (*a*) the number counts by Davidge are somewhat uncertain because of the small area of the survey (1.6 arcmin^2); (*b*) the bolometric correction to the *K*-band flux, which will be used later, is only applicable down to $K \sim 13$; and (*c*) extending the LF to $K \approx 16$, will affect our derived *K*-band luminosity by less than 5%. The *K*-band luminosity of a star at the Galactic center is related to the apparent *K* magnitude by $L_K(L_\odot) = 3.75 \times 10^{5-0.40K}$, where we took a zero magnitude flux density of 670 Jy, $\lambda = 2.2$ μm, $\Delta\lambda = 0.4$ μm, and adopted a distance of 8.5 kpc to the Galactic center. The LF in Baade's window can then be written as

$$\Phi_{BW}(L_K) = 1.73 \times 10^4 \left(\frac{L_K}{L_\odot}\right)^{-1.76} \text{ stars } L_\odot^{-1} \quad \text{for } 1.80 < \frac{L_K}{L_\odot} < 714 , \quad (8)$$

where $\Phi_{BW}(L_K)dL_K$ is the number of stars in the $L_K - L_K + dL_K$ luminosity interval. As a check on the form and the limits of the LF we calculated the total number of giant stars and the *K*-band luminosity in the 604 arcmin^2 area surveyed by DP, and found them to be $\sim 15{,}000$ and $3.5 \times 10^5\ L_\odot$, respectively. The number of K and M giants is in good agree-

ment with the number count of ~17,000 given by DP. The K-band luminosity translates into an average surface brightness of ~13 MJy sr^{-1} in the direction of Baade's window, in good agreement with the value of ~11 MJy sr^{-1} found by the DIRBE.

The LF in equation (8) was derived from observations of Baade's window, so its normalization may not apply to the bulge as a whole. We therefore will adopt the *slope* of the LF as determined from Baade's window to the bulge as a whole, and determine its *normalization* factor from the DIRBE observations. The 2.2 μm bulge luminosity, $L_{K;\,\mathrm{bulge}}$ can be written in terms of the K-band luminosity function as

$$L_{K;\,\mathrm{bulge}} = \int_{L_1}^{L_2} L_K \Phi_{\mathrm{bulge}}(L_K) dL_K \,, \tag{9}$$

where Φ_{bulge} is the LF function of the bulge, and L_1, L_2 are respectively the lower and upper limit of the luminosity function. Using equations (8) and (9), the 2.2 μm luminosity of the bulge can be written as

$$L_{K;\,\mathrm{bulge}} = \mathscr{K} \int_{L_1}^{L_2} \left(\frac{L_K}{L_\odot}\right)^{-0.76} dL_K \tag{10}$$

where $\{L_1, L_2\} = \{1.8\ L_\odot, 714\ L_\odot\}$, and $\mathscr{K}$ is the normalization constant of the bulge LF which can now be written in terms of $L_{K;\,\mathrm{bulge}}$ as

$$\begin{aligned}\mathscr{K}(\mathrm{stars}\ L_\odot^{-1}) &= 0.0654 L_{K;\,\mathrm{bulge}}(L_\odot) \\ &= 2.62 \times 10^7 \ \text{for}\ L_{K;\,\mathrm{bulge}} = 4 \times 10^8\ L_\odot \,. \end{aligned} \tag{11}$$

The bolometric luminosity of the bulge, L_{bol}, is given by

$$L_{\mathrm{bol;\,bulge}} = \int_{L_{K;\min}}^{L_{K;\max}} \xi(L_K) L_K \Phi_{\mathrm{bulge}}(L_K) dL_K \,, \tag{12}$$

where $\xi(L_K)$ is the bolometric correction to the K-band luminosity. Davies, Frogel, & Terndrup (1991) find that the bolometric correction (BC) for the K and M giants in Baade's window is well correlated with their K magnitude over the wide range of $13 < K < 6$. Their expression for the bolometric correction is $\mathrm{BC}(K) = 5.482 - 0.259K - 23.24/K^2$. The BC ranges therefore from 2.0 to 3.3 magnitudes in the ~13 to 6 mag interval (see also Fig. 1 in Frogel & Whitford 1987). It is more convenient to express the bolometric correction in terms of the K-band luminosity. We find that $\xi(L_K) = 5.55(L_K/L_\odot)^{0.194}$, and that the bolometric luminosity of the bulge is

$$\begin{aligned}L_{\mathrm{bol;\,bulge}}(L_\odot) &= 13.3 L_{K;\,\mathrm{bulge}}(L_\odot) \\ &= (5.3 \pm 1.6) \times 10^9\ L_\odot \\ &\qquad \text{for}\ L_{K;\,\mathrm{bulge}} = 4 \times 10^8\ L_\odot \,. \end{aligned} \tag{13}$$

The value of 13.3 derived for the bolometric correction is similar to the crude estimate of ~14.5 derived in § 6.1. This bolometric luminosity is smaller than the value of 1.4×10^{10} $L_\odot$ derived by Maihara et al. (1982) from their 2.4 μm observations of the Galactic center region (the value of 2×10^{10} $L_\odot$ quoted in their paper was presumably calculated for a Galactocentric distance of 10 kpc).

6.3. *The Mass of Giant Stars and the Total Bulge Mass*

The total mass of K and M bulge giants is given in terms of the LF as

$$M_{\mathrm{giants}} = \int_{L_1}^{L_2} M(L_K) \Phi_{\mathrm{bulge}}(L_K) dL_K \,, \tag{14}$$

where $M(L_K)$ is the stellar mass as a function of the K-band luminosity. The stars currently on the giant branch span a narrow range of stellar masses above M_{TO}, the value of the bulge turnoff mass. The absolute V magnitude of the turnoff point in the H-R diagram was recently observed by the Wide Field Camera of the *HST* (Holtzman et al. 1993) who found that $M_V = +4$ (see also Rich 1992 for previous observations). The inferred turnoff mass depends on the assumed stellar metallicities. A large spread in the metallicity would imply a large spread in the progenitor masses. However, the *HST* observations narrowed the spread in metallicities to less than twice solar from $Z = 0$. Stellar isochrones for solar metallicity ($Z = 0.0169$) and metal-rich ($Z = 0.03$) clusters suggest a turnoff mass between 1.20 and 0.90 $M_\odot$, respectively (VandenBerg 1985; VandenBerg & Laskarides 1987). Adopting an average value of $M(L_K) = 1.0\ M_\odot$ for all L_K, we get that the mass of bulge giants is given by

$$\begin{aligned}M_{\mathrm{giants}}(M_\odot) &= 0.054 L_{K;\,\mathrm{bulge}}(L_\odot) \quad \text{for}\ M_{\mathrm{TO}} = 1\ M_\odot \,, \\ &= 2.2 \times 10^7\ M_\odot \qquad \text{for}\ L_{K;\,\mathrm{bulge}} = 4 \times 10^8\ L_\odot \,. \end{aligned} \tag{15}$$

The uncertainty in the mass is about ±40% due to the combined uncertainties in $L_{K;\,\mathrm{bulge}}$ and M_{TO}.

The mass of giant stars comprises only a small fraction of the total mass of the bulge, which is predominantly composed of main sequence (MS) stars. The total mass of main sequence (MS) stars is given by

$$M_{\mathrm{MS}} = \int_{M_0}^{M_{\mathrm{TO}}} M \Psi(M) dM \,, \tag{16}$$

where $\Psi(M)dM$ is the number of stars in the mass interval $M - M + dM$, and M_0 the lower mass limit of the initial mass function $\Psi(M)$. The initial mass function (IMF) can be written as a power law in M, $\Psi(M) \sim M^{-\alpha}$, with $\alpha = 2.35$ for a Salpeter IMF. Writing $\Psi(M) = \Psi(M_{\mathrm{TO}})(M/M_{\mathrm{TO}})^{-\alpha}$, the mass of the bulge becomes

$$M_{\mathrm{MS}} = \Psi(M_{\mathrm{TO}})(M_{\mathrm{TO}})^2 \int_{X_0}^{1} X^{-\alpha+1} dX \,, \tag{17}$$

where $X_0 = M_0/M_{\mathrm{TO}}$. A theoretical expression relating the normalization of the IMF to the total bolometric luminosity L_{bol} of the bulge post-MS population is

$$\Psi(M_{\mathrm{TO}}) = \mathscr{B} \left(\frac{dM_{\mathrm{TO}}}{dt}\right)^{-1} L_{\mathrm{bol}} \,, \tag{18}$$

where $\mathscr{B} \approx 2 \times 10^{-11}\ L_\odot^{-1}\ \mathrm{yr}^{-1}$ is the stellar death rate per unit luminosity (Renzini & Greggio 1990), and

$$\left(\frac{dM_{\mathrm{TO}}}{dt}\right) = \frac{M_{\mathrm{TO}}(M_\odot)}{t(\mathrm{yr})} \left| 0.112 \log\left[t(\mathrm{yr})\right] - 1.338 \right|$$

is an analytical approximation from stellar evolutionary calculations (Renzini & Buzzoni 1986). Equation (18) was derived by noting that (*a*) $\Psi(M_{\mathrm{TO}})\Delta M_{\mathrm{TO}} = N_{\mathrm{RGB}}$, the number of red giants in the M_{TO} to $M_{\mathrm{TO}} + \Delta M_{\mathrm{TO}}$ mass interval that peeled off the main sequence; (*b*) $N_{\mathrm{RGB}} = \mathscr{B} L_{\mathrm{bol}} t_{\mathrm{RGB}}$, where t_{RGB} is the duration time of the red giant phase (Renzini & Greggio 1990); and (*c*) by approximating $\Delta M_{\mathrm{TO}}/t_{\mathrm{RGB}} \approx (dM_{\mathrm{TO}}/dt)$. The time t in the expression for (dM_{TO}/dt) is the turnoff age which is between 5 and 10 billion yr (Holtzman et al. 1993). Adopting a value of $t = 8 \times 10^9$ gives $(dM_{\mathrm{TO}}/dt) = 2.86 \times 10^{-11}\ M_\odot\ \mathrm{yr}^{-1}$. Com-

bining equations (17) and (18), the mass of MS stars can now be written as

$$M_{\rm MS}(M_\odot) = \frac{0.7 M_{\rm TO}(M_\odot)}{\alpha - 2}\left[\left(\frac{M_{\rm TO}}{M_0}\right)^{\alpha-2} - 1\right] L_{\rm bol}(L_\odot)\,,$$
$$= 33 L_{K;\rm bulge} \quad \text{for } \alpha = 2.35 \text{ and } M_0 = 0.1\ M_\odot\,,$$
$$= 1.3 \times 10^{10} \quad \text{for } L_{K;\rm bulge} = 4 \times 10^8\ L_\odot\,. \qquad (19)$$

with an uncertainty of at least 40% due to the determination of the mass of red giants. This photometrically derived mass is in very good agreement with the value of $\sim 1 \times 10^{10}\ M_\odot$ derived by Kent (1992) from dynamical considerations. In terms of the bolometric luminosity we find that the ratio of the dynamically determined mass to the total bolometric luminosity of the bulge is $(M_{\rm dyn}/L_{\rm bol}) \approx 2$, larger than the value of 1 derived by Kent (1992), but the same as the value of 2 ± 0.4 derived by Matsumoto et al. (1982).

7. CONCLUSIONS AND COMPARISON TO PREVIOUS WORK

We have modeled the Galactic bulge morphology and derived its luminosity and mass using the DIRBE observations of its projected surface brightness in the $|l| \leq 10°$, and $|b| \geq 3°$ region at 2.2 μm, and in the $|l| \leq 10°$, and $|b| \geq 2°$ region at 3.5 and 4.9 μm. The main results of the paper, and their relation to previous investigations can be briefly summarized as follows.

Bulge morphology.—(1) The bulge is a bar with its closest edge in the first Galactic quadrant. Even though an axisymmetric oblate spheroid (model G0) provides a reasonable fit to the observed intensity (see Fig. 3*a*), it fails to reproduce the longitudinal asymmetry observed in the DIRBE data (Weiland et al. 1994). This reconfirms the results of Weiland et al. and previous photometric studies of the bulge (Blitz & Spergel 1991), as well as studies of stellar populations and stellar and gas kinematics in the Galactic center region. (2) Triaxial models provide an improved fit to the data, and produce a longitudinal asymmetry in the projected intensity maps. Of the list of triaxial models studied [see eq. (3)], the Gaussian-type models (G1–G3), and the triaxial version of the modified spheroid used by Kent et al. (1991), model E3, provided the best fits to the data. (3) Triaxial models produced axis ratios of $\{x_0{:}y_0{:}z_0\} = \{1{:}0.33 \pm 0.11{:}0.23 \pm 0.08\}$. Thus the bulge resembles a prolate spheroid with a triaxiality, $\mathcal{T} = [1 - (y_0/x_0)^2]/[1 - (z_0/x_0)^2]$, between 0.81 and 0.94. For comparison, Vietri (1986) derived axis ratios of $\{1{:}0.7{:}0.4\}$ from dynamical constraints on model G3. Our notation convention is depicted in Figure 2. (4) Comparison of the results of model E2 with the fit of Whitelock & Catchpole to the population of bulge Mira variables suggests that the *IRAS* selected Mira distribution is significantly flatter than the population of bulge K and M giants. This morphological discrepancy is puzzling considering the widely held view that M stars evolve into Miras. However, the difference in the morphology of these two populations probably arises from the fact that the *IRAS* Miras used in their analysis form an incomplete sample of all Miras with respect to their periods and spatial distribution. (5) The in-plane rotation angle α (see Fig. 2) is between 50° and 80°, the range of values reflecting the variance between the different models. This corresponds to a range of viewing angles (the angle between the solar radius and the bar's major axis) between 10° and 30°. This range is consistent with the value of $16° \pm 2°$ suggested by Binney et al. (1991), and the value of $36° \pm 10°$ suggested by Weinberg (1992a). The models most consistent with Binney et al. are G1 and G2, whereas Weinberg's results favor models G3 and E3. The bar could intrinsically be peanut-shaped but appear boxy because of the nearly end-on viewing angle (Combes & Sanders 1981). (6) The models are consistent with a slight tilt in the bar by an angle $\beta \approx 0.°6$ at 2.2 μm and by $\beta \approx 2°$ at 3.5 and 4.9 μm. However, these tilts are statistically insignificant, and can be accounted for by a nonuniform distribution of foreground stars. (7) A roll can affect the projected intensity of a given functional form. The effect of a roll was most noticeable for model E1, giving an intensity that was initially flattened along the galactic plane a "boxy" appearance.

Bulge luminosity.—(1) The in-band luminosity as determined from a simple integration of the $10° \times 10°$ region around the galactic center is 1.2×10^9, 4.1×10^8, 2.3×10^8, and 4.3×10^7 at 1.25, 2.2, 3.5, and 4.9 μm, respectively. Spatial integration over the volume emissivity corresponding to the various functional forms gives similar values for the luminosities (see Table 4). Most of this emission comes from K and M giants (Arendt et al. 1994). We adopt a nominal value of $(4.0 \pm 1.0) \times 10^8\ L_\odot$ for the 2.2 μm luminosity of the bulge. This value is consistent with the $3.3 \times 10^8\ L_\odot$ derived by Kent et al. (1991) from the 2.4 μm IRT observations. (2) Using the K-band luminosity function and the bolometric correction for bulge K and M giants in the direction of Baade's window, we derived an average bolometric correction of 13.3 for the 2.2 μm band. The total bolometric luminosity $L_{\rm bol}$ of the bulge is then $(5.3 \pm 1.6) \times 10^9\ L_\odot$, smaller than the value of $1.4 \times 10^{10}\ L_\odot$ derived by Maihara et al. (1982) from their 2.4 μm observations of the Galactic center region.

Bulge mass.—Using the *HST* observed bulge turnoff mass and the K-band luminosity function determined in Baade's window, we derived a total mass for the bulge K and M giants of $M_{\rm giants}(M_\odot) = 0.054 L_{K;\rm bulge}(L_\odot)$. The fuel consumption theory of Renzini & Buzzoni (1982) relates $L_{\rm bol}$ of the giants to the total mass of their main-sequence progenitors. Adopting a Salpeter initial mass function extended to a lower mass cutoff of 0.1 $M_\odot$, we derive a total bulge mass of $M_{\rm MS} = (1.3 \pm 0.5) \times 10^{10}\ M_\odot$. This value represents the first photometric determination of the bulge mass and is in good agreement with the dynamic determination of $1 \times 10^{10}\ M_\odot$ (Kent 1992; Matsumoto et al. 1982).

We thank Leo Blitz, Michael Feast, Michael Rich, David Spergel, Allen Sweigart, Martin Weinberg, Patricia Whitelock, and HongSheng Zhao for helpful discussions, Adolfo Figueroa-Vinas for advice on the numerical fitting procedure, Tom Statler for his suggestion to include a roll in the model, and Ned Wright and other members of the *COBE* Science Working Group for their general comments on the manuscript. The National Aeronautics and Space Administration/Goddard Space Flight Center (NASA/GSFC) is responsible for the design, development, and operation of the *Cosmic Background Explorer* (*COBE*), under the scientific guidance of the *COBE* Science Working Group.

REFERENCES

Arendt, R. G., et al. 1994, ApJ, 425, L85
Bahcall, J. 1986, ARA&A, 24, 577
Bahcall, J. N., Schmidt, M., & Soneira, R. 1982, ApJ, 258, L23
Bard, Y. 1974, Nonlinear Parameter Estimation (Orlando: Academic)
Becklin, E. E., & Neugebauer, G. 1968, ApJ, 151, 145
Binney, J., & Gerhard, O. 1993, in Back to the Galaxy, ed. S. S. Holt & F. Verter (New York: AIP), 87
Binney, J. J., Gerhard, O. E., Stark, A. A., Bally, J., & Uchida, K. I. 1991, MNRAS, 252, 210
Blanco, V. 1988, AJ, 95, 1400
Blanco, V. M., & Trendrup, D. M. 1989, AJ, 98, 843
Blitz, L. 1993, in Back to the Galaxy, ed. S. S. Holt & F. Verter (New York: AIP), 98
Blitz, L., & Spergel, D. N. 1991, ApJ, 379, 631
Chen, W., Gehrels, N., & Diehl, R. 1994, ApJ, submitted
Combes, F., Debbasch, F., Friedli, D., & Pfenniger, D. 1990, A&A, 233, 82
Combes, F., & Sanders, R. H. 1981, A&A, 96, 164
Davidge, T. J. 1991, ApJ, 380, 116
Davies, R. L., Frogel, J. A., & Terndrup, D. M. 1991, AJ, 102, 1729
De Poy, D. L., Terndrup, D. M., Frogel, J. A., Atwood, B., & Blum, R. 1993, AJ, 105, 2121
de Vaucouleurs, G. 1948, Ann. d'Astrophys., 11, 247
de Zeeuw, T. 1985, MNRAS, 216, 273
———. 1992, in The Stellar Populations of Galaxies, ed. B. Barbuy & A. Renzini (Dordrecht: Kluwer), 51
Eadie, W. T., Drijard, D., James, F. E., Roos, M., & Sadoulet, B. 1971, Statistical methods in Experimental Physics (North-Holland: Amsterdam)
Frogel, J. A. 1988, ARA&A, 26, 51
Frogel, J. A., & Whitford, A. E. 1987, ApJ, 320, 199 (FW)
Frogel, J. A., Whitford, A. E., & Rich, R. M. 1984, AJ, 89, 1536
Habing, H. J., Olnon, F. M., Chester, T., Gillett, F., Rowan-Robinson, M., & Neugebauer, G. 1985, A&A, 152, L1
Hauser, M. G. 1993, in Back to the Galaxy, ed. S. S. Holt & F. Verter (New York: AIP), 201
Hernquist, L. 1990, ApJ, 356, 359
Holtzman, J. A., et al. 1993, AJ, 106, 1826
Kent, S. M. 1992, ApJ, 387, 181
Kent, S. M., Dame, T. M., & Fazio, G. 1991, ApJ, 378, 131
Liszt, H. S., & Burton, W. B. 1980, ApJ, 236, 779
Maihara, T., Oda, N., Sugiyama, T., & Okuda, H. 1978, PASJ, 30, 1
Matsumoto, T., et al. 1982, in The Galactic Center, ed. G. Riegler & R. Blandford (New York: AIP), 48
Nakada, Y., Deguchi, S., Hashimoto, O., Izumiura, H., Onaka, T., Sekiguchi, K., & Yamamura, I. 1991, Nature, 353, 140
Paczyński, B., Stanek, K. Z., Udalski, A., Szymański, M., Kałuzny, J., Kubiak, M., Mateo, M., & Krzeminski, W. 1994, ApJ, 435, L113
Press, W. H., Flannery, B. P., Teukolsky, S. A., & Vetterling, W. T. 1986, Numerical Recipes (Cambridge: Cambridge Univ. Press)
Raha, N., Sellwood, J. A., James, R. A., & Kahn, F. D. 1991, Nature, 352, 411
Renzini, A., & Buzzoni, A. 1986, in Spectral Evolution of Galaxies, ed. C. Chiosi & A. Renzini (Dordrecht: Reidel), 195
Renzini, A., & Greggio, L. 1990, in Bulges of Galaxies (ESO Conf. Workshop Proc. No. 35), 47
Rich, R. M. 1992, in The Stellar Population of Galaxies, ed. B. Barbuy & A. Renzini (Dordrecht: Kluwer), 29
Rieke, G. H., & Lebofsky, M. J. 1985, ApJ, 288, 618
Rowan-Robinson, M., & Chester, T. 1987, ApJ, 313, 413
Ruelas-Mayorga, R. A. 1991, Rev. Mexicana Astron. Astrof., 22, 27
Sanders, R. H., & Lowinger, T. 1972, AJ, 77, 292
Sellwood, J. A. 1993, in Back to the Galaxy, ed. S. S. Holt & F. Verter (New York: AIP), 133
Shlosman, I., Frank, J., & Begelman, M. C. 1989, Nature, 338, 45
Stanek, K. Z., Mateo, M., Udalski, A., Szymański, M., Kałuzny, J., & Kubiak, M. 1994, ApJ, 429, L73
Statler, T. S. 1987, ApJ, 321, 113
VandenBerg, D. A. 1985, ApJS, 58, 711
VandenBerg, D. A., & Laskarides, P. G. 1987, ApJS, 64, 103
Vietri, M. 1986, ApJ, 306, 48
Wainscoat, R. J., Cohen, M., Volk, K., Walker, H. J., & Schwartz, D. E. 1992, ApJS, 83, 111
Weiland, J., et al. 1994, ApJ, 425, L81
Weinberg, M. D. 1992a, ApJ, 384, 81
———. 1992b, ApJ, 392, L67
Whitelock, P. 1993, in Galactic Bulges, ed. H. deJonghe & H. J. Habing (Dordrecht: Kluwer), 39
Whitelock, P., & Catchpole, R. 1992, in The Center, Bulge, and Disk of the Milky Way, ed. L. Blitz (Dordrecht: Kluwer), 103